Impact of common sea surface temperature anomalies on global drought and pluvial frequency

Kirsten L. Findell and Thomas L. Delworth

Geophysical Fluid Dynamics Laboratory

Princeton, NJ

Draft

23 March 2008

For submission to *Journal of Climate*,

Special Issue for the Clivar Drought Working Group

Abstract

Climate model simulations run as part of the Clivar Drought Working Group initiative were analyzed to determine the impact of three patterns of sea surface temperature (SST) anomalies on drought and pluvial frequency and intensity around the world. The three SST forcing patterns include a global pattern similar to the background warming trend, a pattern in the Pacific, and a pattern in the Atlantic. Five different global atmospheric models were forced by fixed SSTs to test the impact of these SST anomalies on droughts and pluvials relative to a climatologically-forced control run.

The five models generally yield similar results in the locations of droughts and pluvials for each given SST pattern. In all of the simulations, areas with an increase (decrease) in the mean drought index values tend to also show an increase in the frequency of pluvial (drought) events. Additionally, areas with more frequent extreme events also tend to show higher intensity extremes. The cold Pacific anomaly increases drought occurrence in the United States and southern South America, and increases pluvials in Central America, and northern and central South America. The cold Atlantic anomaly increases drought occurrence in southern Central America, northern South America, and Central Africa, and increases pluvials in central South America. The warm Pacific and Atlantic anomalies generally lead to reversals of the drought and pluvial increases described with the corresponding cold anomalies. More modest impacts are seen in other parts of the world. The impact of the trend pattern is generally more modest than that of the two other anomaly patterns.

1. Introduction

The Clivar Drought Working Group was established “to facilitate progress on the understanding and prediction of long-term (multi-year) drought over North America and other drought-prone regions of the world, including an assessment of the impact of global change on drought processes” (U.S. Clivar Drought Working Group Prospectus, 12 December 2006). From this directive, a multi-model comparison project was initiated, in which all the participating models were forced with the same set of three large-scale patterns of sea surface temperature (SST) anomalies. The goal of the project was to assess the role of these commonly occurring SST patterns in driving and/or exacerbating drought.

The goal of this paper is to document the impact of the three primary SST patterns on drought and pluvial frequency and intensity around the world, as determined by the multi-model mean of these experiments. Differences between the model responses will also be discussed. In the next section, we will discuss broad aspects of the five participating models. In Section 3 we will define the drought measures used in this study. Results from the Pacific, Atlantic, and Trend-based experiments will be discussed in Section 4, prior to some discussion in Section 5 and concluding statements in Section 6.

2. Model descriptions and experimental design

The idealized SST experiments were performed with five different global atmospheric climate models:

1. the Geophysical Fluid Dynamics Laboratory (GFDL) used the AM2.1 (Delworth et al., 2006; GAMDT, 2004; Milly and Shmakin, 2002);
2. the Global Modeling Assimilation Office (GMAO) of National Aeronautics and Space Administration (NASA) Goddard Space Flight Center (GSFC) used the NASA NSIPP1 (Bacmeister et al., 2000);
3. the Community Climate System Model (CCSM) Climate Variability Working Group at the National Center for Atmospheric Research (NCAR) used the NCAR CAM3.5 (http://www.ccsm.ucar.edu/models/atm-cam/; Neale et al., 2008; Oleson et al., 2008; Stockli et al., 2008);
4. the Climate Group of Lamont-Doherty Earth Observatory (LDEO) at the Columbia University used the NCAR CCM3 (Kiehl et al, 1998); and
5. the Climate Prediction Center (CPC) of the National Center for Environmental Prediction (NCEP) used the NCEP Global Forecast System (GFS; Campana and Caplan, 2005).

The five models will be referred to by the names GFDL, NSIPP, CAM3.5, CCM3, and GFS. Each of the models is documented in the references listed above, and in Schubert et al. (2009) which provides an overview of the Working Group's initiative.

2a. SST forcing fields

Figure 1a shows the SST climatology derived from the Hadley Centre data spanning the years 1901-2004 (HadISST; Rayner et al., 2003). A rotated empirical orthogonal function (EOF) analysis (Kaiser, 1958) identified the three leading patterns of interannual SST variability as a pattern resembling the linear trend of global SST, a warm-phase pattern in the Pacific, and a warm-phase pattern in the Atlantic. These patterns represent 27.2%, 20.5% and 5.8% of the global SST variance. Although the third EOF explains such a small percent of the global variance, it does explain up to 70% of the local variance in the region of the intertropical convergence zone (ITCZ) during northern summer. The analysis was restricted to ice-free points.

These patterns were scaled by the standard deviations of the respective principal component time series. The Pacific and Atlantic patterns were multiplied by twice the standard deviation of their respective principal components to create patterns similar to those observed in years of great extremes in these basins (Figures 1c and 1d), while the linear warming trend was multiplied by one standard deviation to maintain a pattern with historical relevance (as opposed to a future warming pattern; Figure 1b). The robustness of this trend pattern will be discussed in Section 4e. These anomalies were then added to the climatological seasonal cycle of SST and used as the new boundary condition of the model's simulation.

2b. Experimental design

Each modeling group ran a series of eight experiments with all possible combinations of a warm and cold Pacific and Atlantic forcing, in addition to the control experiment (Table 1). When referring to these combination experiments, we will use the notation of Table 1: e.g., PcAw refers to the experiment with both the cold Pacific and the warm Atlantic anomaly patterns added to the climatological SSTs of the control experiment; PwAn refers to the experiment with the warm Pacific and a neutral (or no) Atlantic pattern added to the climatology. Four of the modeling groups ran the experiments for more than 50 years, while the GFS experiments were run for 37 years. The last 50 years are used when available; the last 36 years are used with the GFS results.

In none of the experiments discussed in this paper is the SST response in the atmosphere permitted to feedback to the ocean and alter SSTs. Thus, while these experiments provide clear insight into the way SST anomalies can alter regional climate properties, they overlook the interesting question of further feedbacks and coupling to the SST fields. Such a study would require a full dynamic coupled model with an interactive ocean, beyond the scope of the present intercomparison project. Further discussion of the limitations of fixed-SST experiments is provided in Section 5.

3. Drought and pluvial definitions

Drought can be defined in many ways, with many different spatial and temporal frames of reference. As a review of drought definitions by Wilhite and Glanz (1985) makes clear, there is not—and cannot be—one universal definition of drought, given the different time and space scales of interest in various meteorological, agricultural, and hydrologic resource issues. Precipitation (or lack thereof) is the primary factor in drought considerations, but temperature, radiation, the growth stage of vegetation, the ability of the vegetation to access groundwater, and many other factors play critical roles in the development or abatement of drought in the real world. The Drought Monitor (http://drought.unl.edu/dm) is a tool for tracking and displaying the magnitude and spatial extent of droughts within the United States, and it is founded on the assumption that no single index is suitable for all purposes or for all regions; maps are produced on a weekly basis after fusing objective data from a suite of drought-related indices and subjective data from on-the-ground experts in regions throughout the country (Svoboda et al., 2002).

We will rely on two indicators of drought and pluvial occurrence in this paper: (1) precipitation deciles as an indicator of meteorological drought, and (2) the Supply-Demand Drought Index (SDDI) as an indicator of longer-term drought. Both indices were justified in their original publications as improvements over the Palmer Drought Severity Index (PDSI; Palmer, 1965). The PDSI was a landmark development in drought research because it was the first water-budget-based index: it incorporated antecedent precipitation, moisture supply, and moisture demand into a hydrologic accounting system (Heim, 2002). It was widely adapted to regions far from its original development zone in the Great Basin of the United States, despite Palmer's own warnings against such extrapolation (Heim, 2002). Although no drought index has proven as popular as the PDSI, many studies have analyzed its weaknesses (e.g., Alley, 1984), and others have developed improved versions (e.g., the self-calibrating PDSI of Wells et al., 2004; the modified PDSI of Mo and Chelliah, 2006). Few recent studies claim that the PDSI is well-suited to global analysis, and its continued usage in global studies is typically justified on the basis of its prevalence in past research.

Precipitation deciles were chosen as the meteorological measure of drought in the Australian Drought Watch System in 1992 (White and O'Meagher, 1995). This index was more advantageous than others (particularly the PDSI) for a number of reasons including (1) the simplicity of the necessary data (precipitation would be needed for most drought indicies; this required nothing else), (2) the lack of dependence on information regarding crop types and features, and (3) deciles are applicable to any data distribution (not just normally distributed data) and easily allow one to focus on extreme events (Gibbs and Maher, 1967). The use of precipitation deciles is limited, however, by the failure to account for the impact of temperature or radiation as a driver of evapotranspiration, and by the failure to account for the cumulative impact of prolonged spells of extreme precipitation (low or high values).

Deciles are sometimes used with additional criteria to determine when a drought is over (e.g., if the precipitation total for the past three months is in or above the eighth decile; Keyantash and Dracup, 2002), though such criteria are not used in this study. Keyantash and Dracup (2002) gave rainfall deciles the highest evaluation score among six meteorological drought indices (PDSI among them) considered in their study of data from the state of Oregon. Here we will define drought in a given grid cell as months with precipitation below the 20%-level of the control run (in the bottom two deciles or below the minimum observed value in the control run), and pluvials as months with precipitation above the 80%-level of the control run (in or above the top two deciles).

Keyantash and Dracup (2002) considered five hydrological drought indices and five agricultural drought indices in their comparative study, but all of them are less than ideal for this model intercomparison because of their dependence on soil moisture and/or streamflow. Though soil moisture is clearly a critical factor in real-world droughts, modeled soil moisture is highly dependent on the land surface scheme of the given model and should not be taken as a volumetric measure of actual soil moisture. More importantly, soil moisture from different land surface schemes is reported for different depth levels and relative to different soil porosities and transmissivities. This makes it difficult to calculate soil moisture-dependent drought indices in a consistent manner when considering a suite of models. Streamflow reporting is similarly model-dependent, making streamflow-dependent drought indices unsuitable for a model intercomparison.

The SDDI was first suggested by Rind et al. (1990) as an alternative to the PDSI. It is the difference between the supply of moisture (precipitation, P) and the atmospheric demand for moisture (potential evapotranspiration, E_P). The SDDI has a few significant advantages over the PDSI. First, the index is tied to soil moisture through the evaporative demand, but it does not rely directly on the modeled value of soil moisture. Additionally, there are no grid-specific empirical coefficients to estimate. Its definition is similar in structure to that of the PDSI. First, a difference between the modeled value of $(P - E_P)$ and the monthly climatological value is calculated:

$$d = P - E_P - (P - E_P)_{c\lim},$$

where the climatology is determined from each model's control simulation. Then a "moisture anomaly index" is determined:

$$Z = d / \sigma,$$

where σ is the interannual standard deviation in the monthly $(P - E_P)$ series from the control run climatology. Finally, the cumulative nature of drought is included in the final index through the equation:

$$SDDI(i) = 0.897 \ \ SDDI(i-1) + Z(i).$$

The constant value of 0.897 was chosen by Rind et al. (1990) to mimic the PDSI.

One of the beneficial qualities of the SDDI is the easy-to-understand notion of supply versus demand. However, the demand side of the equation has many potential definitions, and it depends on atmospheric conditions, soil water availability, and vegetation type and growth stage. The concept of potential evaporation was first discussed in 1948 (Thornthwaite, 1948) with the idea of defining some measure of atmospheric demand for moisture if soil moisture availability was not restricted and the vegetation covering over a large area was uniform. Numerical definitions stemming from this concept are plentiful, varied, and empirical. Some E_P definitions require only temperature information, while others require temperature and net radiation, and still others require these variables along with canopy conductance estimates for a specific vegetation type. Given the empirical nature of these equations, it is important to keep in mind that these relationships could change as climate changes. Thus, the E_P definition used here in SDDI calculations should be taken as an indicator of atmospheric moisture demand which may be sensitive to climatic conditions.

Our SDDI calculations make use of the radiation-based method of Priestly and Taylor (1972) for the calculation of E_P:

$$E_p = \frac{\alpha_{PT}\left[s(T_a)\right]R_{net}}{\rho_w \lambda_v \left[s(T_a)+\gamma\right]},$$

where $\alpha_{PT} = 1.26$ was determined empirically from data over both water and saturated land surfaces, R_{net} is net radiation at the surface, T_a is air temperature, ρ_w is the mass density of water, λ_v is the latent heat of vaporization, γ is the psychrometric constant, and $s(T_a)$ is the slope of the relation between saturation vapor pressure (e_{sat}) and air temperature:

$$s(T) = \frac{de_{sat}(T)}{dT} = \frac{25083}{(T+237.3)^2}\exp\left(\frac{17.3T}{T+237.3}\right).$$

Though we believe that precipitation deciles and the SDDI are adequate indicators of large-scale changes in surface conditions, we are fully cognizant of the reality that no index is a perfect measure of drought or pluvials in all regions of the world.

4. Results

We begin our exploration of the results by taking an in-depth look at the Cold Pacific experiment (PcAn) with the GFDL model as a way of detailing the methodologies used in this work. We will then look at results of the PcAn and the PnAw experiment with all five models as well as the multi-model mean to show some of the differences between the models. Subsequent results will only include plots of the multi-model mean (MMM).

4a. Cold Pacific Experiment

Figure 2 shows some results of the Cold Pacific experiment with the GFDL model. Mean precipitation differences (Figure 2a) highlight the same regions of change as indicated by mean SDDI differences (Figure 2b). Results are shown over land only since the SDDI is a quantity with little relevance to the ocean where the "supply" part of the index is always unlimited. In both plots, differences are shaded only where they are statistically significant at the 95% level according to the modified *t*-test of von Storch and Zwiers (1999; the test is modified to account for autocorrelation within the time series). Both plots show regions of decreases in the mean values in the central United States and southern South America, and to a lesser extent in Alaska and central Asia. Regions of increases in the means occur in southern Central America and north- and central-eastern South America (including Amazonia), and to a lesser extent in Indonesia, Australia, and the Arabian peninsula. The similarity between plots 2a and 2b is a reflection of the SDDI being driven primarily by precipitation. The differences between these plots indicate that SDDI is generally a more sensitive index than precipitation deciles. This is likely a result of the two primary differences between the two indices: the SDDI is dependent on temperature and radiation, in addition to precipitation, and the SDDI has some accounting for the cumulative nature of drought.

The second row of Figure 2 highlights regions with increased drought occurrence as measured by the average number of months per year with precipitation below the 20^{th} percentile level of the control run (Figure 2c), and by the average number of months per year with SDDI below -2.0 (Figure 2d). By definition, each grid cell in the control run has 2.4 months/year below the 20^{th} percentile precipitation threshold. The SDDI value of -2.0 marks a similar threshold: grids cells in the control run have values below this threshold on average 2.3 months/year. Grid cells with fewer than 3.0 months/year below the respective thresholds are not shaded in Figure 2c or 2d. The regions of increased drought frequency shaded in Figures 2c and 2d are largely coincident with regions of decreases in the mean precipitation (Figure 2a) and the mean SDDI (Figure 2b).

These measures of drought occurrence—monthly precipitation or SDDI compared to a climatological norm—do not account for the fact that some months are more important than others in drought considerations. In many cases, a relative dry spell during an already dry month can be ameliorated by normal rainfall during the rainiest time of the year, while rainfall deficits during the rainy season are much more difficult to make up. However, given the global nature of this analysis, we felt it was important to include all months of the year. For a more detailed analysis of individual regions, a seasonal approach might be warranted.

The bottom row of Figure 2 provides similar information about the occurrence of pluvials in this Cold Pacific experiment. Figure 2e shows slight increases in the average number of months per year with precipitation exceeding the 80th percentile of the control run. These areas are largely coincident with regions with increased mean precipitation (Figure 2a). Figure 2f shows locations with increased occurrence of SDDI values greater than 2.0. These areas are largely coincident with areas of increases in mean SDDI (Figure 2b).

Though the locations of increased drought and pluvial occurrence are generally consistent between the precipitation deciles (Figures 2c and 2e) and the SDDI calculations (Figure 2d and 2f), the average number of months per year in an extreme is much higher in the SDDI plots than in the precipitation decile plots. As discussed above in regard to the mean precipitation and SDDI differences, these differences in drought and pluvial occurrence stem from the additional climatic information included in the SDDI calculation and from the short-term (individual months) perspective of deciles, versus the cumulative nature of the SDDI. This relationship between the two measures of drought is seen in all experiments and with all models. Consequently, we will only show SDDI values in subsequent plots.

Figures 3 and 4 show the SDDI-based drought and pluvial frequency for the cold Pacific experiment for each of the five participating models, as well as for the multi-model mean. The results of the multi-model mean (MMM) shown in Figures 3f and 4f closely match the results from the GFDL model discussed above in regard to Figure 2, and shown again in Figures 3a and 4a. These impacts include increased drought frequency in the continental United States and southern South America, and to a lesser extent in southern Europe into Central Asia and along the southeastern coast of Asia. Additionally, we see increased pluvial frequency in southern Central America, northern and central South America, and to a lesser extent Australia, Arabia, India, and South Africa. All of the models show these same general results, with notable variations in the spatial extent of the responses and the intensity of the increases. Most notably, the CAM model shows increased pluvial frequency throughout northern Africa, extending into the Mediterranean region. This pushes the European and Central Asian drought response in CAM further north than in GFDL, NSIPP, and CCM3. GFS also shows the European region of increased drought farther north than the MMM. In general, peak values of drought and pluvial frequency are highest in the CAM results and lowest in the GFS results.

Figures 5 and 6 show a measure of drought and pluvial intensity for the cold Pacific experiment for each of the five models and the MMM: the average value of the SDDI when the SDDI exceeds the -2.0 and +2.0 thresholds. For all the models in general, and particularly in the MMM, the regions of increased drought occurrence (Figure 3) tend to coincide with regions of increased drought intensity (Figure 5). Similarly, Figures 4 and 6 show that the highest SDDI intensities occur where high SDDI values occur more frequently. Additionally, comparison of Figures 5 and 6 shows that high end extremes tend to be larger in magnitude than low end extremes. This is likely a reflection of the long tail on the high end and the zero-limit on the low end of precipitation distributions.

4b. Warm Atlantic Experiment

Figure 7 shows that all five models indicate increased drought activity in the continental United States in response to the Warm Atlantic experiment (PnAw), though details of the responses certainly differ. The MMM shows a broad region with increased drought frequency, though the peak is only 4 months/year in drought, as opposed to 8 months/year in response to the PcAn forcing. Other regions showing increased drought frequency include central South America and modest increases in southern Europe, Alaska, southern Australia, and scattered sections of southeast Asia. CCM3 shows a very strong response in Africa, extending into the Mid-East and much of Asia, but these increases are not borne out in the MMM.

Four of the five models show a very strong increase in pluvial activity in southern Central America and northern-most South America, extending across the Atlantic and into the Guinea Coast of Africa in response to PnAw. GFS shows a much more modest response to this anomaly than the other models. CAM's response is the most intense in number of months/year in pluvial, and the extent of the response is much broader in Africa than the other models show. The MMM also shows a modest increase in pluvial across much of northern Europe and Asia, and in Indonesia.

4c. Warm Pacific Experiment

Figures 9 and 10 show MMM SDDI-based drought and pluvial frequencies for each of nine experiments shown in Table 1. The central figures indicate that only a handful of grid points in the control run have SDDI values lower than -2.0 or higher than 2.0 for more than 3 months/year. Figures 9d and 10d are the same as Figure 3f and 4f, respectively, showing drought and pluvial frequency for the cold Pacific experiment. Figures 9f and 10f show that the warm Pacific experiment generally leads to a reversal of the cold Pacific pattern: where the cold Pacific increases drought, the warm Pacific increases pluvials and vice-versa. In both cases, the number of months/year tend to be slightly higher on the pluvial side: for example, Figure 10f shows peak values of over 9 months/year in the central U.S. in pluvial with the warm Pacific forcing, while the cold Pacific forcing results in peak values of 8 months/year in the same location (Figure 9d). There are additional differences in the spatial signatures in areas with less pronounced increases. The cold Pacific experiment showed modest drought increases in southern Europe extending into central Asia, for example. The warm Pacific experiment shows pluvial increases over a much broader portion of Europe, but few grid points with values above 3 months/year in central Asia. There are additional differences around the Indian Ocean: the cold Pacific experiment leads to increased pluvial in the Arabian peninsula and India, while the warm Pacific experiment leads to increased droughts along the east coast of Africa. Nevertheless, to first order, the warm Pacific and the cold Pacific anomalies lead to opposite drought and pluvial impacts in most regions of the world.

4d. Cold Atlantic Experiments

The warm and cold Atlantic forcings also lead to generally opposite results, though the slightly stronger response on the pluvial side is more evident in these two experiments. Figures 9b and 10b show the drought and pluvial frequency with the cold Atlantic forcing, and Figures 9h and 10h show the same plots for the warm Atlantic forcing (identical to Figures 7f and 8f). The cold Atlantic forcing leads to increases in drought occurrence in southern Central America, northern South America, and a narrow region along the Guinea Coast of West Africa and into the Congo region. Increases in pluvials are seen in central South America, extending south into the Parana region. Modest pluvial increases are seen in the continental U.S. and northern Mexico. Modest drought increases are seen in much of northern-most Asia. This is largely a reversal of the patterns discussed in Section 4b in regard to the warm Atlantic experiment.

4e. Pacific/Atlantic Combination Experiments

Drought occurrence results for the four combination experiments (PcAc, PwAc, PcAw, and PwAw) are shown in the four corner subplots of Figure 9. To first order, the results of the combination experiments most closely resemble their Pacific counterpart with a neutral Atlantic, indicating that for most parts of the globe, the Pacific forcing is more dominant than the Atlantic. This is not entirely surprising, given the much broader spatial footprint and maximum intensity of the Pacific pattern (Figure 1c) compared to the Atlantic pattern (Figure 1d). Nevertheless, the Atlantic impacts are still substantial. In fact, Atlantic and Pacific impacts along the Guinea Coast and in the Congo region of Africa seem about equal in strength, with drought frequency maximized in the warm

Pacific/cold Atlantic (PwAc) experiment (Figure 9c). Though pluvial frequencies are maximized in the cold Pacific/warm Atlantic (PcAw) experiment (Figure 10g), all of the experiments with a warm Atlantic increase pluvial frequency in these regions, with the broadest area of response occurring in the warm Pacific/warm Atlantic (PwAw) experiment (Figure 10i).

For much of North and South America, the Atlantic and Pacific patterns work in opposition: drought occurrences are maximized in North America and southern South America in PcAw. Pluvial occurrences in these regions are maximized in PwAc. For southern Central America and northern South America, drought occurrences are maximized in PwAc, and pluvial occurrences are maximized in PcAw. The Amazonian region is the exception: here the two forcings work in parallel, with drought occurrences maximized in PwAw and pluvial occurrences maximized in PcAc.

Impacts in Indonesia and neighboring islands are largely independent of the Atlantic condition, with all warm Pacific experiments leading to increased drought frequency and all cold Pacific experiments leading to increased pluvial frequency. These patterns generally extend south into Australia, though the values are much lower (up to 12 months/year in extreme in Indonesia versus 3-6 months/year in Australia).

Impacts are modest in Europe and Asia, with MMM values of months/year in an extreme rarely surpassing 4. This modest impact is seen over the largest area with droughts in PcAc and with pluvials in PwAw.

4e. Trend Experiments

Figure 11 shows the MMM results of the experiment with the warm linear trend pattern shown in Figure 1b added to the climatology shown in Figure 1a. Both the drought plot (Figure 11a) and the pluvial plot (Figure 11b) show that the impact of the warm trend experiment is generally much smaller than the impact of the other two anomaly patterns.

The analysis of Vecchi and Soden (2007) and Vecchi et al. (2008) showed significant dependence of the SST trend pattern on the original SST dataset. They show that the cooling along the equator in the eastern Pacific shown in Figure 1b is not present in the SST trend pattern derived from the Smith and Reynolds (2004) dataset. This is an indication that not all features of the SST trend pattern may be robust and that drought and pluvial results from these experiments forced with the Hadley-based trend patterns may differ from experiments forced by different SST trend patterns.

5. Discussion

It is worth noting that the SST forcing patterns used in this study were not derived in order to maximize drought or pluvial impacts in any particular location. On the contrary, the forcing patterns were determined from an unbiased EOF analysis aimed at isolating the leading patterns of variability in the global oceans. The results presented in this paper are largely in agreement with previous studies on the impact of Pacific and Atlantic forcing of precipitation and of drought in various regions of the world. Hoerling and Kumar (2003), Schubert et al. (2004), Seager et al. (2005), Herweijer and Seager (2008) and many others provide compelling evidence for the strong global-scale forcing from the tropical Pacific. Each of these studies shows that drought in much of the United States in particular and throughout the midlatitudes in general tends to occur when the eastern tropical Pacific is cooler than normal (La Nina conditions). Hoerling and Kumar (2003) (and others) extend this result to show that a warm Atlantic further exacerbates midlatitude drought conditions. Though the anomaly patterns they discuss are different from the ones used in this study, particularly in the western Pacific, our results with the PcAw experiment largely confirm their conclusion that cold Pacific and warm Atlantic conditions are best-suited to mid-latitude drought. Seager et al. (2003) explain that this impact is driven by changes in the locations of the subtropical jets and the effects these jets have on the eddy-driven mean meridional circulation.

McCabe et al. (2004) find an association between multidecadal variations in Atlantic SSTs and precipitation and surface temperature changes in the United States, and Sutton and Hodson (2005) report similar findings for both Europe and the United States. Warm Atlantic SSTs were found to lead to temperature increases in both regions (with larger magnitudes and larger regions of significance in the U.S.), precipitation reductions in the U.S., and precipitation increases in Europe. Thus, impacts of Atlantic SST variations on drought inferred from their findings would be more substantial in the U.S. than in Europe. This is consistent with findings presented here.

Much research has focused on the region encompassing southern Central America, the Caribbean Sea, and northeastern Brazil. In the results presented here, the Pacific influence in the Caribbean and northern South America is of uniform sign over a region extending south to about 18-20ºS latitude (warm Pacific increases drought occurrence, Figure 9f; cold Pacific increases pluvial occurrence, Figure 10d). The Atlantic influence in this region extends southward to about 5ºS latitude (warm Atlantic increases pluvials, Figure 10h; cold Atlantic increases droughts, Figure 9b). North of 5ºS, SST anomalies of opposing signs are associated with the greatest propensity to drought or pluvial: a cold Pacific and a warm Atlantic are most conducive to pluvials (Figure 10g), while a warm Pacific and a cold Atlantic are most conducive to droughts (Figure 9c). From about 5 to 20ºS, anomalies of the same sign are associated with the greatest propensity to drought or pluvial: cold SSTs in both basins yields most pluvials (Figure 10a), and warm SSTs in both basins yields most droughts (Figure 9i). These results are confirmed by a wide range of studies (e.g., Hastenrath, 1979; Enfield and Alfaro, 1999; Giannini et al., 2001).

Studies about rainfall in the Sahel and the Guinea Coast of Africa indicate the importance of SST conditions adjacent to the region (Giannini et al., 2003). This is consistent with our finding that the Atlantic impacts more strongly on this region than the Pacific. However, other research indicates that the cross-equatorial SST gradient in the Atlantic is critical to precipitation conditions in this region (Fontaine and Janicot, 1996), while still other research highlights the importance of uniform warming to drying in the Sahel (particularly with the GFDL model CM2.0; Held et al., 2005). Drought occurrence in the runs reported here does increase in the Sahel in the warm Trend experiment in the GFDL model, with a range of 3-6 months/year in drought in the Sahel (not shown). The MMM, however, shows that much of the region has less than 3 months/year in drought (Figure 11a).

Fundamental research on the ENSO phenomenon indicate that rainfall in Indonesia and the surrounding areas broadly termed Oceania is strongly linked to SSTs in the tropical Pacific, with warm conditions in the eastern tropical Pacific yielding more rain than normal in that area and far less rain than normal in Oceania (e.g., Hendon, 2003). This is consistent with the picture of increased drought in Indonesia in our MMM results in each of the warm Pacific experiments, almost independent of the Atlantic condition (Figures 9c, f, and i), and increased pluvials in Indonesia in each of the cold Pacific experiments (Figures 10a, d, and g).

Research on the connections between Australian rainfall and ENSO events in the Pacific indicate a high degree of temporal variability in the relationship (Cai et al., 2001; Suppiah, 2004). Indeed, Cai et al. (2001) show that though there is typically a strong association between drought in northeastern Australia and warm conditions in the eastern tropical Pacific, this relationship has reversed on a number of occasions, most notably during the period from 1931-45. They note that this weakening in the ENSO-rainfall relationship occurs when the linearly detrended global mean temperature is particularly high, though they do not determine a cause for the weakening. Rainfall in southwest Western Australia has been shown to be dependent on interactions between Indian Ocean SSTs and wind fields (England et al., 2006). However, other research indicates that fixed-SST experiments are of limited use in areas where rainfall has a strong impact on the temperature of the underlying ocean (e.g., Lau and Nath, 2000; Wang et al., 2005; Bracco et al., 2007). Wang et al. (2005) show that the feedbacks between the atmosphere and the Indian ocean cannot be neglected in simulation of the Asian-Pacific summer monsoon rainfall, and Bracco et al. (2007) try to determine which areas of the tropical oceans must interact with the atmosphere to properly capture the relationship between ENSO and the Asian summer monsoon. These limitations of fixed-SST experiments on the simulation of rainfall in areas impacted by the Indian Ocean clearly extend to our discussion of droughts and pluvials in these regions. Further research on drought occurrence in the areas surrounding the Indian Ocean should be conducted with a fully coupled ocean model.

6. Conclusions

Climate model simulations run as part of the Clivar Drought Working Group initiative were analyzed to determine the impact of three SST anomaly patterns on drought and pluvial frequency and intensity around the world. The three patterns are a global pattern reflecting the observed warming trend, a Pacific pattern and an Atlantic pattern. Five different atmospheric models (GFDL, NSIPP, CAM3.5, CCM3, GFS) were coupled to fixed SST oceans to test the impact of these SST anomalies on droughts and pluvials relative to a climatologically-forced control run.

The five models generally yield similar results in the locations of droughts and pluvials. In all of the simulations, areas with an increase (decrease) in the mean drought index values tend to also show an increase in the frequency of high-end (low-end) extreme drought index values. Additionally, areas with more frequent extremes also tend to show higher intensity extremes. Though all models are in general agreement with the MMM in broad terms, CAM3.5 tends to be more sensitive than the other models in Africa, and peak values of drought and pluvial frequency tend to be higher with CAM3.5 and lower with GFS than with the other models.

Areas of greatest drought and pluvial sensitivity under these forcing scenarios include most of the Americas. MMM results show that drought frequencies are highest in the continental U.S., Mexico, and southern South America when the Pacific is cold and the Atlantic is warm (PcAw). Pluvial frequencies in these regions are highest with the opposite oceanic forcings (PwAc). Southern Central America and northern South America respond in the opposite way to these forcings, with drought maximized in PwAc experiments and pluvials maximized in PcAw experiments. Indonesia is strongly affected by Pacific conditions, with a cold Pacific yielding increases in pluvials and a warm Pacific yielding increases in droughts. More modest impacts are seen in Europe and

Australia, with Australia following Indonesia’s patterns but with substantially reduced frequencies. The largest areas of modest impact in Europe occur with increased droughts in PcAc and increased pluvials in PwAw. Results for areas strongly impacted by Indian Ocean SSTs should be interpreted with caution given the importance of ocean-atmosphere feedbacks in this region and the limitations of fixed SST experiments.

These idealized experiments are a useful aid to improve our understanding of the factors contributing to drought in regions all around the world, however, it is important to remember that these experiments are indeed idealizations and not perfect reflections of the real world. Nevertheless, the substantial agreement between these five very different models on the locations of increased drought and pluvial frequency under each of the experimental scenarios indicates that these results are likely to be robust.

Acknowledgments

This work was carried out as part of a U.S. CLIVAR drought working group activity supported by NASA, NOAA, and NSF to coordinate and compare climate model simulations forced with a common set of idealized SST patterns. The authors would like to thank NASA's Global Modeling and Assimilation Office (GMAO) for making the NSIPP1 runs available, the Lamont-Doherty Earth Observatory of Columbia University for making their CCM3 runs available, NOAA's Climate Prediction Center (CPC)/Climate Test Bed (CTB) for making the GFS runs available, NOAA's Geophysical Fluid Dynamics Laboratory (GFDL) for making the AM2.1 runs available, the National

Center for Atmospheric Research (NCAR) for making the CAM3.5 runs available, and the Center for Ocean Land Atmosphere (COLA) and the University of Miami's Rosenstiel School of Marine and Atmospheric Science for making the CCSM3.0 coupled model runs available. We would also like to thank Yana Malysheva for guaranteeing that the GFDL data were consistent with the CMOR protocol, and Paul Ginoux and Gabriel Vecchi for their helpful comments on the manuscript.

References

Alley, William M., 1984: “The Palmer Drought Severity Index: Limitations and Assumptions.” *J. Climate and Applied Meteorology*, **23**, 1100-1109.

Bacmeister J., P. J. Pegion, S. D. Schubert, and M. J. Suarez, 2000: “*An atlas of seasonal means simulated by the NSIPP 1 atmospheric GCM.*” Vol. 17. NASA Tech. Memo. 104606, Goddard Space Flight Center, Greenbelt, MD, 194 pp.

Bracco, Annalisa, Fred Kucharski, Franco Molteni, Wilco Hazeleger, and Camiel Severijns, 2007: “A recipe for simulating the interannual variability of the Asian summer monsoon and its relation with ENSO.” *Climate Dynamics*, **28**, 441-460.

Cai, W., P.H. Whetton, and A.B. Pittock, 2001: “Fluctuations of the relationship between ENSO and northeast Australian rainfall.” *Climate Dynamics*, **17**, 421-432.

Campana, K. and P. Caplan, Editors, 2005: “*Technical Procedure Bulletin for T382 Global Forecast System.*” (http://www.emc.ncep.noaa.gov/gc_wmb/Documentation/TPBoct05/T382.TPB.FINAL.htm)

Delworth et al., 2006. “GFDL's CM2 global coupled climate models - Part 1: Formulation and simulation characteristics.” *J. Clim.*, **19**(5), 643-674.

Enfield, David B. and Eric J. Alfaro, 1999: “The Dependence of Caribbean Rainfall on the Interaction of the Tropical Atlantic and Pacific Oceans.” *J. Clim.*, **12**, 2093-2103.

England, M.H., C.C. Ummenhofer, and A. Santoso, 2006: “Interannual Rainfall Extremes over Southwest Western Australia Linked to Indian Ocean Climate Variability.” *J. Clim.*, **19**, 1948-1969.

Fontaine, Bernard and Serge Janicot, 1996: “Sea Surface Temperature Fields Associated with West African Rainfall Anomaly Types.” *J. Clim.*, **9**, 2935-2940.

Giannini, A., J.C.H. Chiang, M.A. Cane, Y. Kushnir, and R. Seager, 2001: “The ENSO Teleconnection to the Tropical Atlantic Ocean: Contributions of the Remote and Local SSTs to Rainfall Variability in the Tropical Americas.” *J. Clim.*, **14**, 4530-4544.

Giannini, A., R. Saravanan, and P. Chang, 2003: “Oceanic Forcing of Sahel Rainfall on Interannual to Interdecadal Time Scales.” *Science*, **302**, 1027-1030.

The GFDL Global Atmospheric Model Development Team, 2004. “The New GFDL Global Atmosphere and Land Model AM2-LM2: Evaluation with Prescribed SST Simulations.” *J. Clim.*, **17**(24), 4641-4673.

Hastenrath, Stefan, 1979: “On Modes of Tropical Circulation and Climate Anomalies.” *J. Atmos. Sci.*, **35**, 2222-2231.

Hendon, Harry H., 2003: “Indonesian Rainfall Variability: Impacts of ENSO and Local Air-Sea Interaction.” *J. Clim.*, **16**, 1775-1790.

Heim, Richard R., Jr, 2002. “A Review of Twentieth-Century Drought Indices Used in the United States.” *Bull. American Meteor. Soc.*, **83**(8), 1149-1165.

Held, I. M., T. L. Delworth, J. Lu, K. L. Findell, and T. R. Knutson, 2005: “Simulation of Sahel drought in the 20th and 21st centuries.” *Proceedings of the National Academy of Sciences*, **102(50)**, 17891-17896.

Herweijer, Celine and Richard Seager, 2008: “The global footprint of persistent extra-tropical drought in the instrumental era.” *Int. J. Climatol.* DOI: 10.1002/joc.1590.

Hoerling, Martin and Arun Kumar, 2003: “The Perfect Ocean for Drought.” *Science*, **299**, 691-694.

Keyantash, John and John A. Dracup, 2002. “The Quantification of Drought: An Evaluation of Drought Indices.” *Bull. American Meteor. Soc.*, **83**(8), 1167-1180.

Kiehl, J.T., J.J. Hack, G. Bonan, B.A. Boville, D. Williamson and P. Rasch, 1998. “The National Center for Atmospheric Research Community Climate Model: CCM3.” *J. Clim.*, **11**, 1131-1149.

Lau, Ngar-Chang and Mary Jo Nath, 2000: “Impact of ENSO on the Variability of the Asian-Australian Monsoons as Simulated in GCM Experiments.” *J. Clim.*, **13**, 4287-4309.

McCabe, Gregory J., Michael A. Palecki, and Julio L. Betancourt, 2004: “Pacific and Atlantic Ocean influences on multidecadal drought frequency in the United States.” *Proceedings of the National Academy of Sciences*, **101(12)**, 4136-4141.

Milly, P. C. D., and A. B. Shmakin, 2002. “Global modeling of land water and energy balances. Part I: The land dynamics (LaD) model.” *J. Hydromet.*, **3**(3), 283-299.

Mo, Kingtse C. and Muthuvel Chelliah, 2006: “The Modified Palmer Drought Severity Index Based on the NCEP North American Regional Reanalysis.” *J. Applied Meteorology and Climatology*, **45**, 1362-1375.

Neale, R.B., J.H. Richter, and M. Jochum, 2008: “The Impact of Convection on ENSO: From a Delayed Oscillator to a Series of Events.” *J. Climate*, **21**,5904-5924.

Oleson, K. W., G.-Y. Niu, Z.-L. Yang, D.M. Lawrence, P. E. Thornton, P. J. Lawrence, R. Stockli, R. E. Dickinson, G. B. Bonan, S. Levis, A. Dai and T. Qian, 2008: "Improvements to the Community Land Model and their impact on the hydrological cycle." *J. Geophys. Res.*, **113**, G01021, doi:10.1029/2007JG000563.

Palmer, Wayne, 1965: "Meteorological Drought." *Research Paper No. 45*, U.S. Weather Bureau, Washington, D.C.

Priestley, C.H.S. and R.J. Taylor, 1972: "On the Assessment of Surface Heat Flux and Evaporation Using Large-Scale Parameters." *Mon. Wea. Rev.*, **100**(2), 81-92.

Rind, D., R. Goldberg, J. Hansen, C. Rosenzweig, and R. Ruedy, 1990. "Potential Evapotranspiration and the Likelihood of Future Drought." *J. Geophys. Research*, **95**(D7), 9983-10004.

Seager, R., N. Harnik, Y. Kushnir, W. Robinson, and J. Miller, 2003: "Mechanisms of Hemispherically Symmetric Climate Variability." *J. Clim.*, **16**, 2960-2978.

Seager, R., Y. Kushnir, C. Herweijer, N. Naik and J. Velez, 2005. "Modeling tropical forcing of persistent droughts and pluvials: 1856-2000." *J. Clim.*, **18**, 4068-4091.

Schubert, Siegfried D., Max J. Suarez, Philip J. Pegion, Randal D. Koster, and Julio T. Bacmeister, 2004: "On the Cause of the 1930s Dust Bowl." *Science*, **303**, 1855-1859.

Schubert et al., 2009. "A USCLIVAR Project to Assess and Compare the Responses of Global Climate Models to Drought-Related SST Forcing Patterns: Overview and Results." Submitted to *J. Clim.*

Smith, Thomas M. and Richard W. Reynolds, 2004: "Improved Extended Reconstruction of SST (1854-1997)." *J. Clim.*, **17**, 2466-2477.

Stockli, R., D. M. Lawrence, G.-Y. Niu, K. W. Oleson, P. E. Thornton, Z.-L. Yang, G. B. Bonan, A. S. Denning, and S. W. Running, 2008: "Use of FLUXNET in the Community Land Model development." *J. Geophys. Res.*, **113**, G01025, doi:10.1029/2007JG000562.

Suppiah, Ramasamy, 2004: "Trends in the Southern Oscillation Phenomenon and Australian Rainfall and Changes in their Relationship." *Inter. J. Climotol.*, **24**, 269-290.

Sutton, Rowan T. and Daniel L.R. Hodson, 2005: "Atlantic Ocean Forcing of North American and European Summer Climate." *Science*, **309**, 115-118.

Svoboda, Mark, Doug LeComte, Mike Hayes, Richard Heim, Karin Gleason, Jim Angel, Brad Rippey, Rich Tinker, Mike Palecki, David Stooksbury, David Miskus, and Scott Stephens, 2002. “The Drought Monitor.” *Bull. American Meteor. Soc.*, **83**(8), 1181-90.

Vecchi, Gabriel A. and Brian J. Soden, 2007: “Global Warming and the Weakening of the Tropical Circulation.” *J. Clim.*, **20**, 4316-4340.

Vecchi, G.A., A. Clement, and B.J. Soden, 2008: “Examining the Tropical Pacific’s Response to Global Warming.” *EOS*, **89**(9), 81-83.

Von Storch, H. and F.W. Zwiers, 1999: *Statistical Analysis in Climate Research.* Cambridge University Press, Cambridge, UK.

Wang, Bin, Qinghua Ding, Xiouhua Fu, In-Sik Kang, Kyung Jin, J. Shukla, and Francisco Doblas-Reyes, 2005: “Fundamental challenge in simulation and prediction of summer monsoon rainfall.” *Geophys. Research Letters*, **32**, L15711, doi:10.1029/2005GL022734.

Wells, Nathan, Steve Goddard, and Michael J. Hayes, 2004: “A Self-Calibrating Palmer Drought Severity Index.” *J. Clim.*, **17**, 2335-2351.

White, D.H. and B. O'Meagher. 1995. "Coping with exceptional droughts in Australia." *Drought Network News*, **7**(2), 13–17.

Wilhite, Donald A. and Michael H. Glanz, 1985: "Understanding the Drought Phenomenon: The Role of Definitions." *Water International*, **10**, 111-120.

Tables

	Cold Pacifc	Neutral Pacifc	Warm Pacific
Cold Atlantic	PcAc	PnAc	PwAc
Neutral Atlantic	PcAn	PnAn (Control)	PwAn
Warm Atlantic	PcAw	PnAw	PwAw

Table 1: Suite of nine idealized experiments performed by each modeling group.

Figures

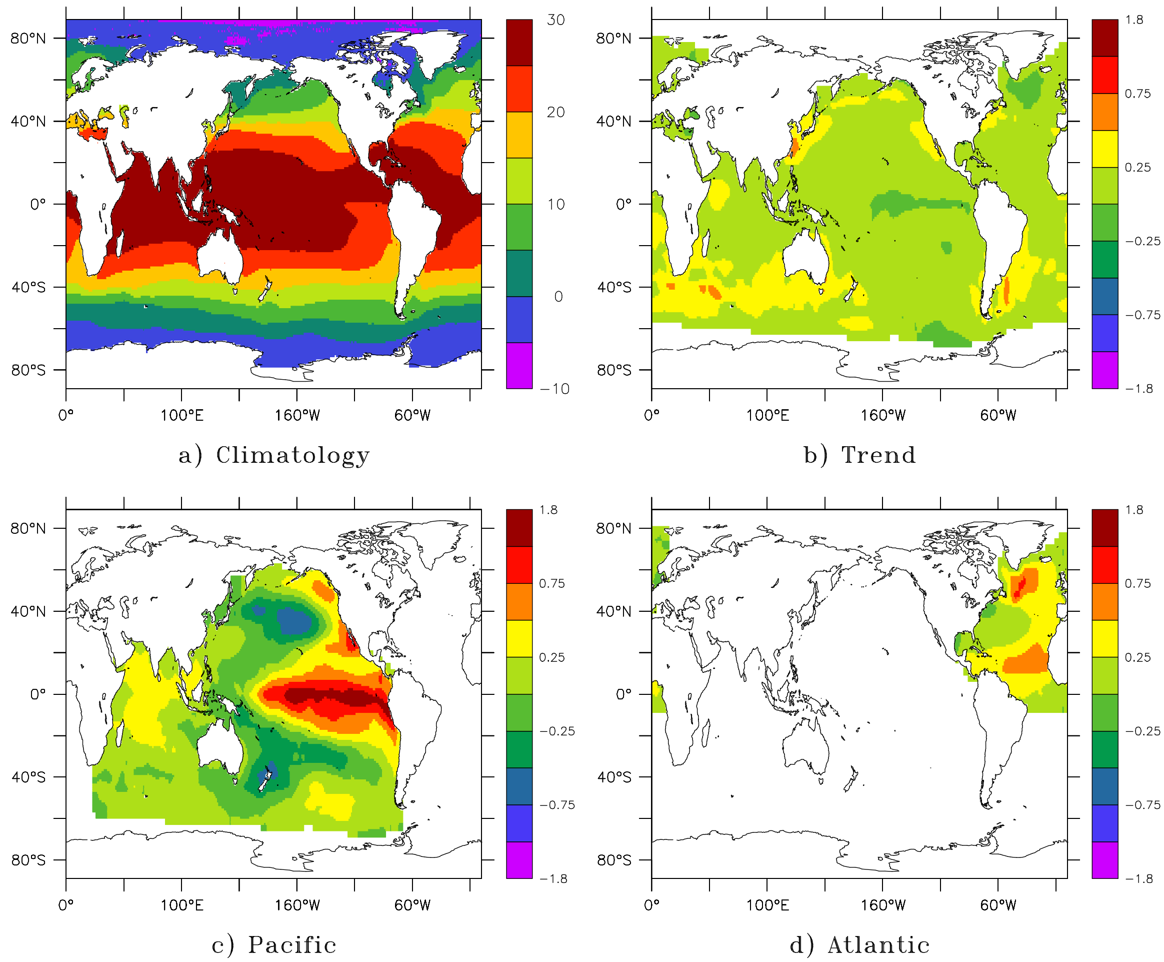

Figure 1: SST forcing patterns: (a) climatology derived from the Hadley Centre dataset spanning the years 1901-2004; (b) warming trend anomaly; (c) Pacific warm-phase anomaly; and (d) Atlantic warm-phase anomaly.

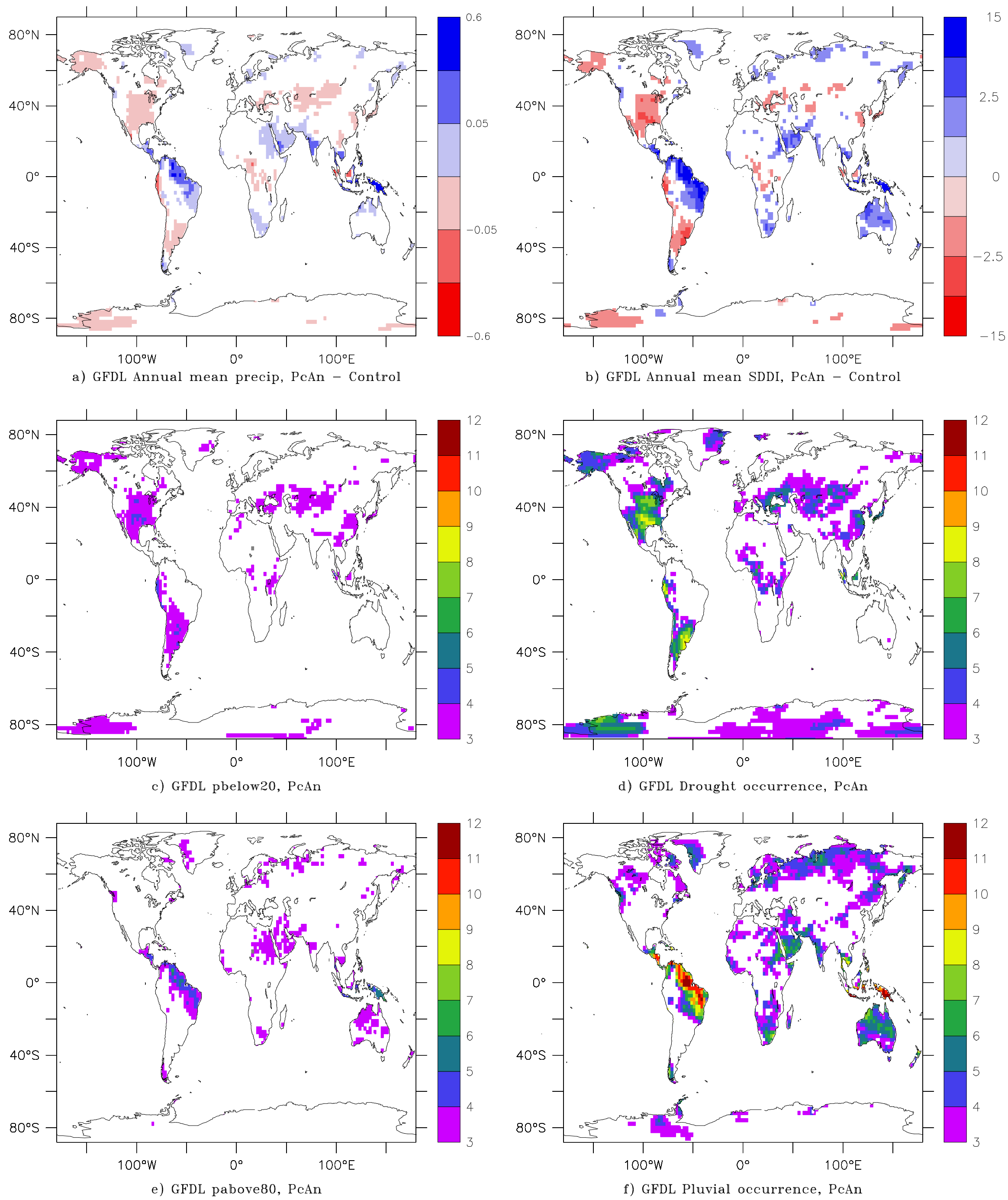

Figure 2: Results of the Cold Pacific experiment (PcAn) with the GFDL model: a) mean precipitation differences from Control run, shaded where significant at the 95% level; b) mean SDDI differences from the Control run, also shaded where significant at the 95% level; c) average number of months/year with precipitation below the 20th percentile of the Control run; d) average number of months/year with SDDI below -2.0; e) average

number of months/year with precipitation above the 80th percentile of the Control run; f) average number of months/year with SDDI above 2.0.

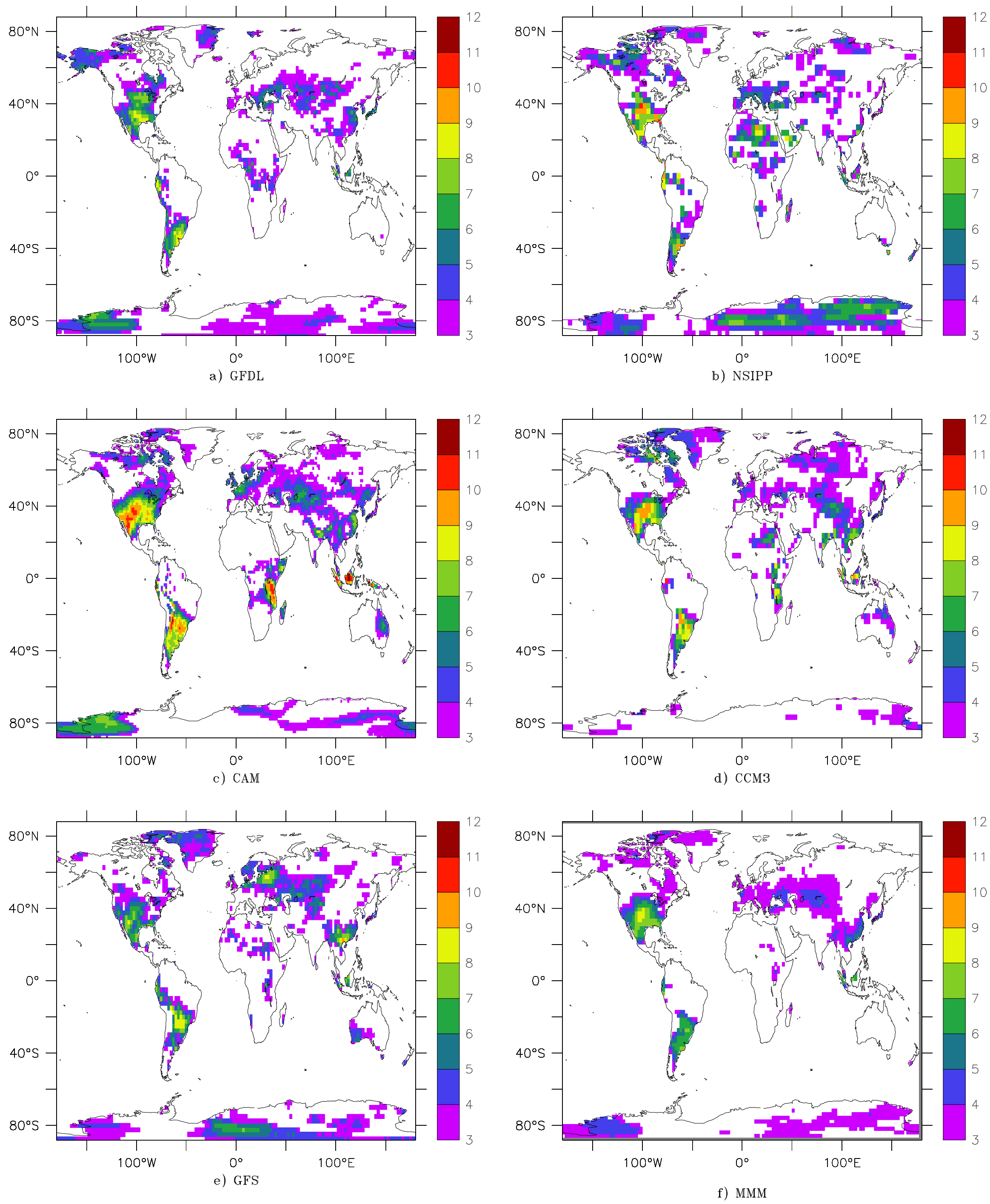

Figure 3: Average number of months per year in drought (SDDI < -2.0), relative to each model's control run, for the cold Pacific experiment: a) GFDL, b) NSIPP, c) CAM, d) CCM3, e) GFS, and f) Multi-model mean (MMM).

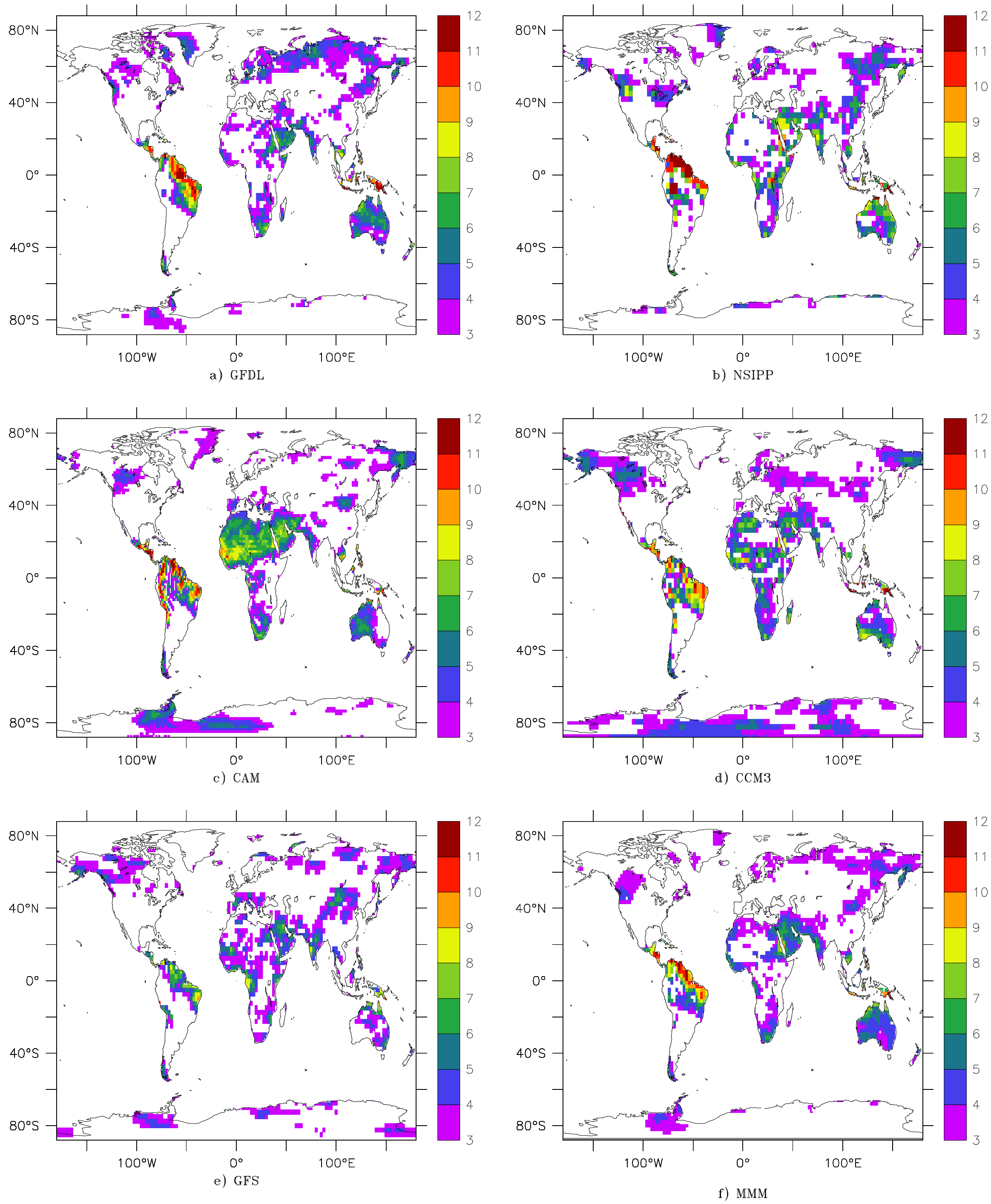

Figure 4: As in Figure 3, but for pluvial occurrence (SDDI > 2.0) with the cold Pacific experiment.

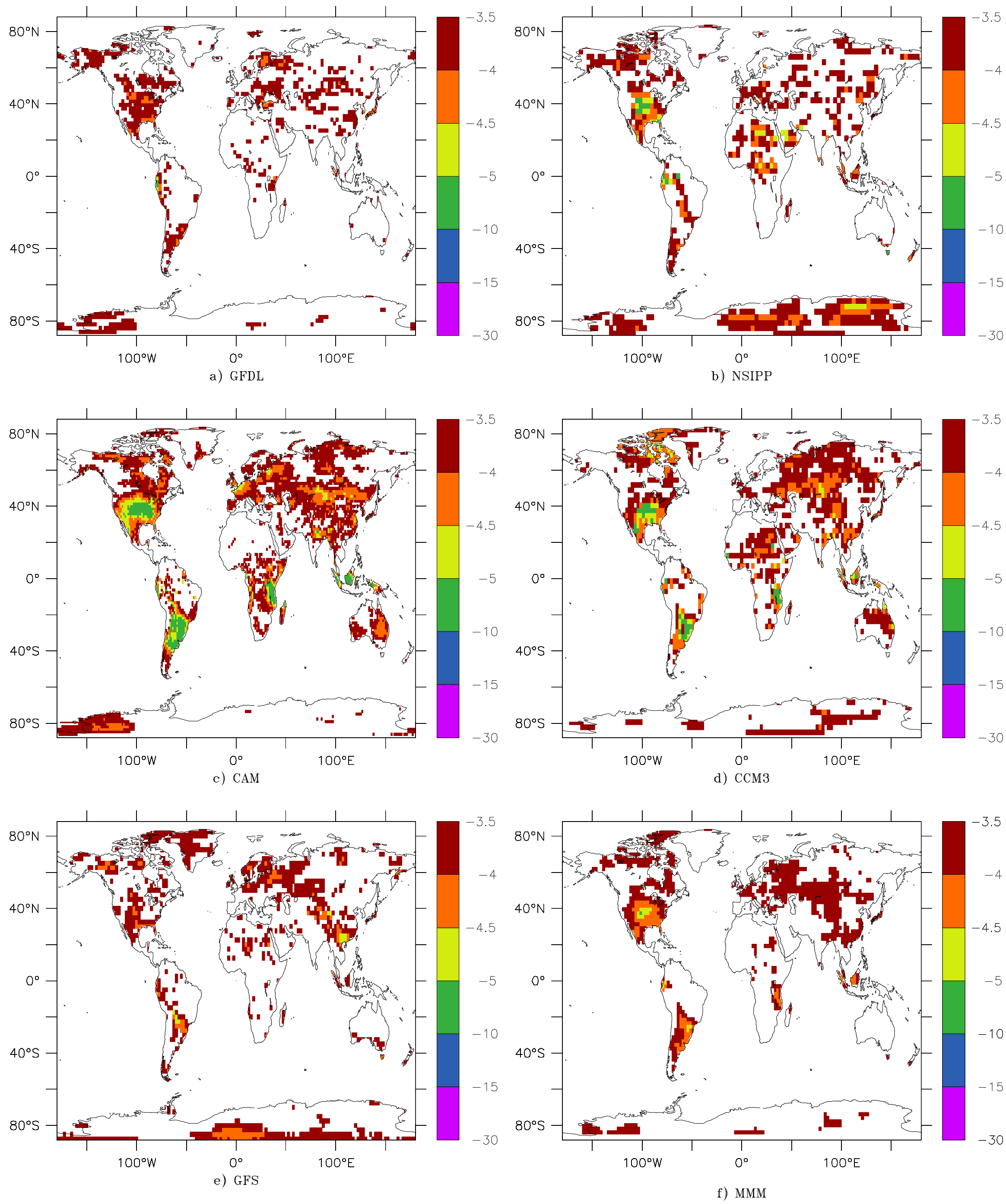

Figure 5: Drought intensity in the cold Pacific experiment, as measured by the mean SDDI value during times of drought (when SDDI < -2.0).

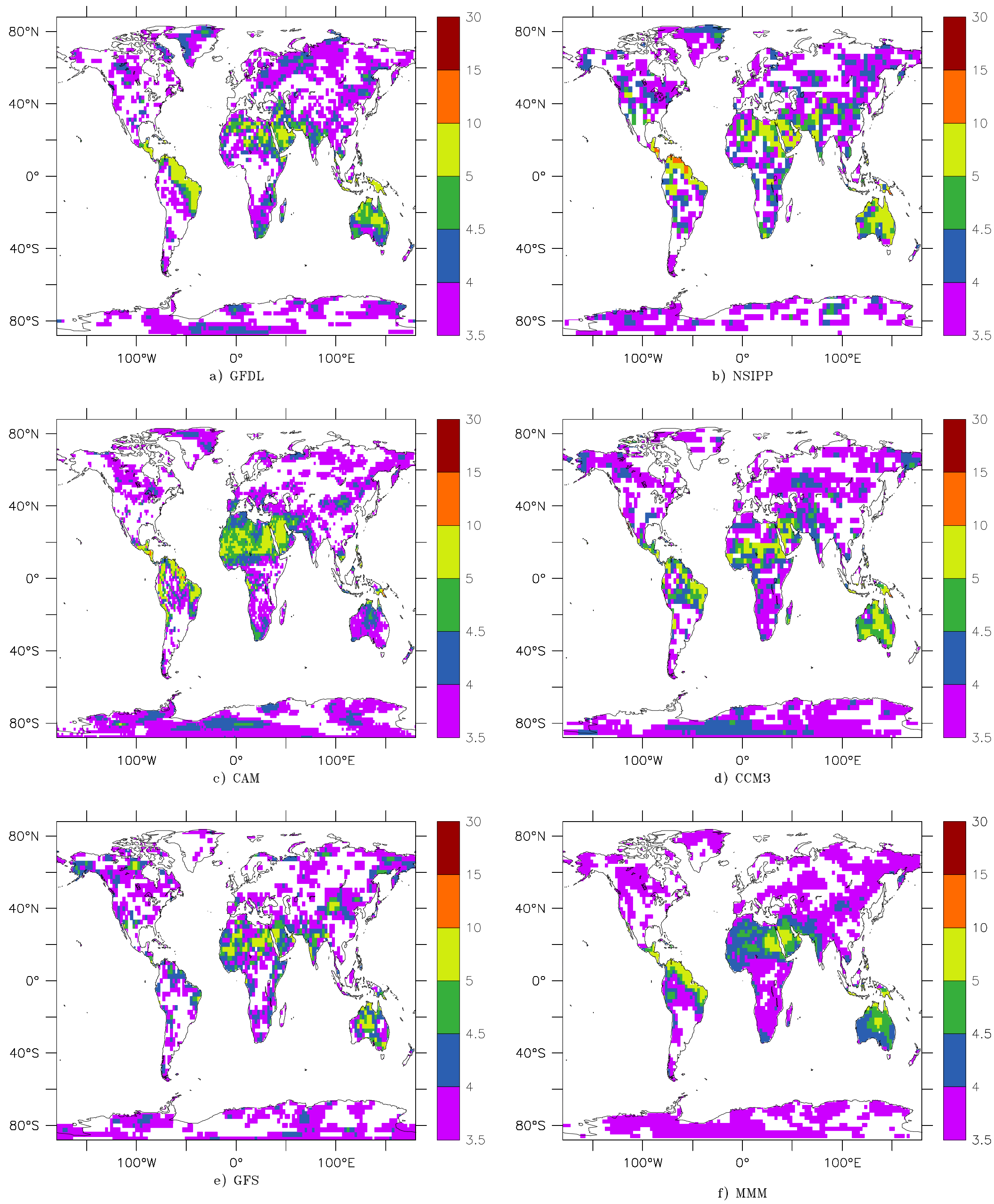

Figure 6: Pluvial intensity in the cold Pacific experiment, as measured by the mean SDDI value during pluvials (when SDDI > 2.0).

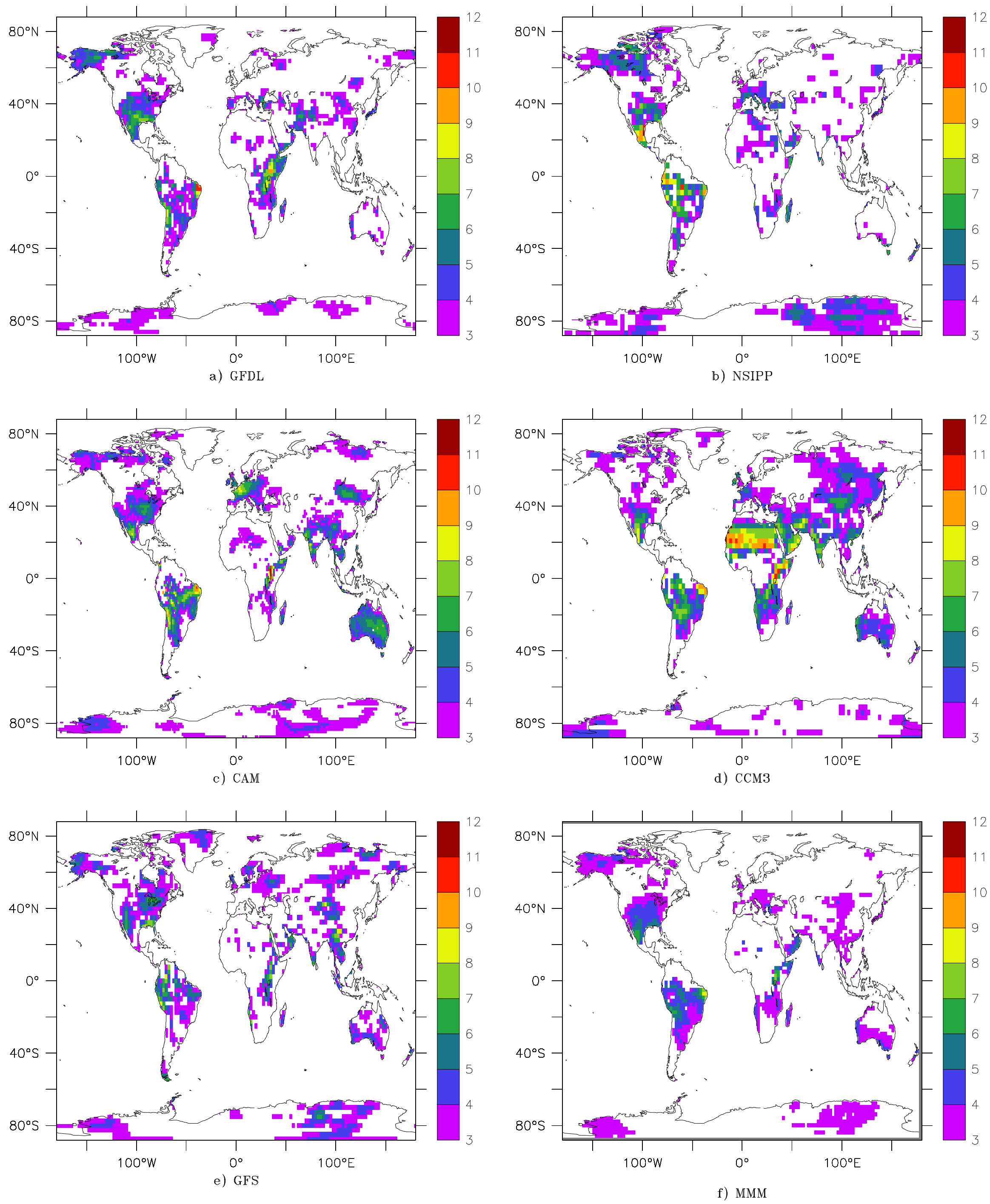

Figure 7: Drought occurrence in the warm Atlantic experiment, as in Figure 3.

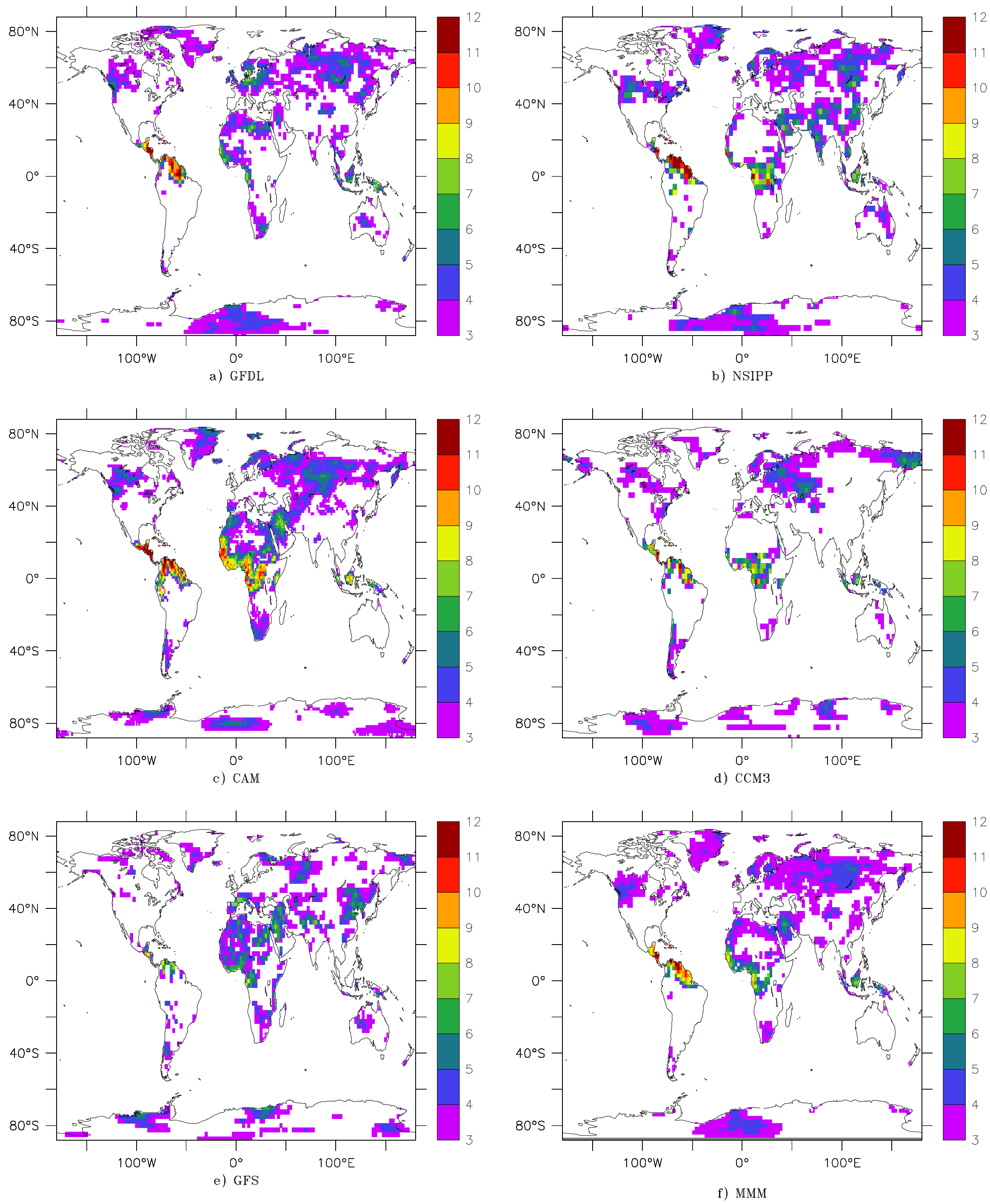

Figure 8: As in Figure 7, but for pluvial occurrence (SDDI > 2.0).

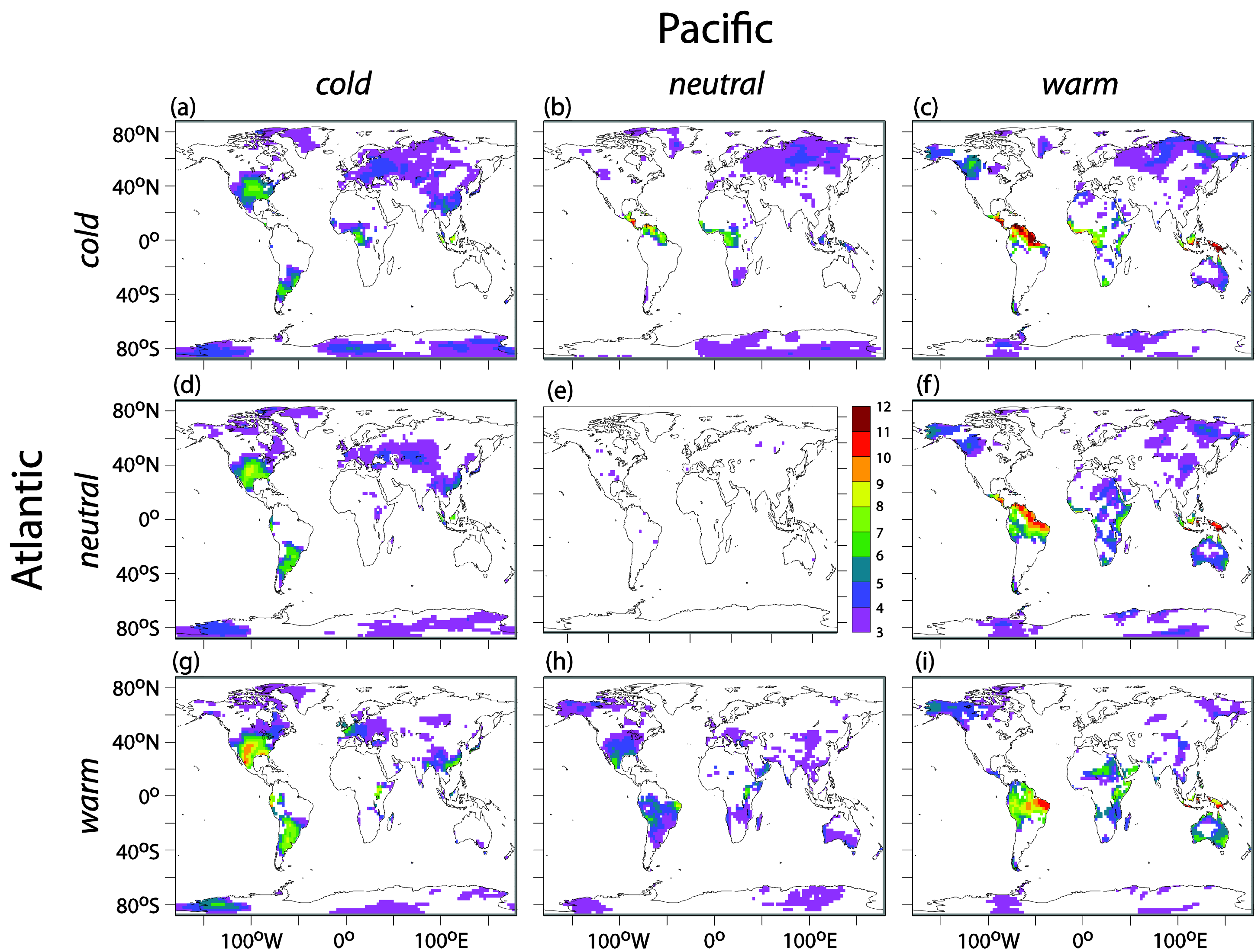

Figure 9: Multi-model mean drought occurrence (average number of months/year with SDDI < -2.0) for nine experiments: a) PcAc, b) PnAc, c) PwAc, d) PcAn, e) PnAn (Control), f) PwAn, g) PcAw, h) PnAw, i) PwAw.

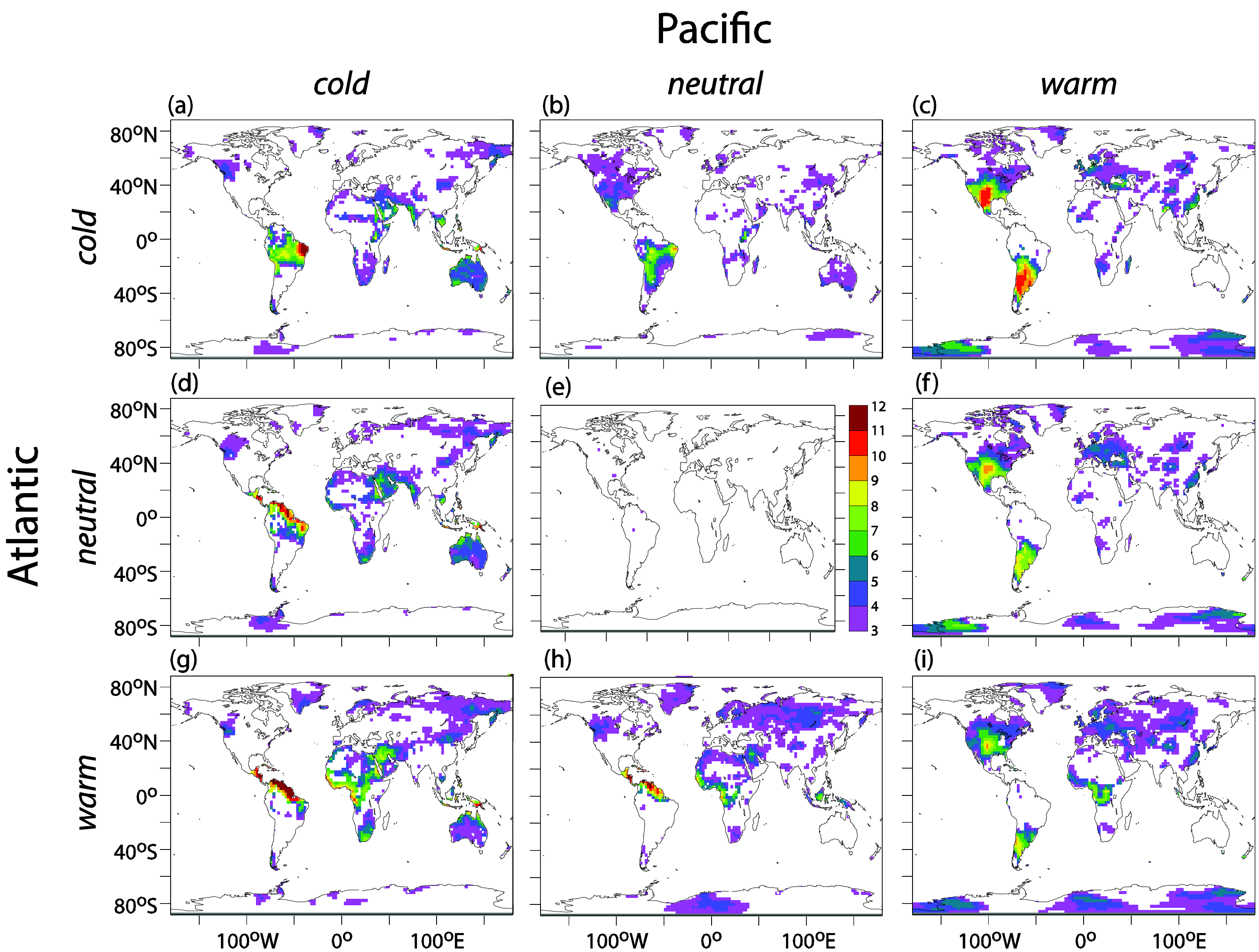

Figure 10: As in Figure 9, but for pluvial occurrence.

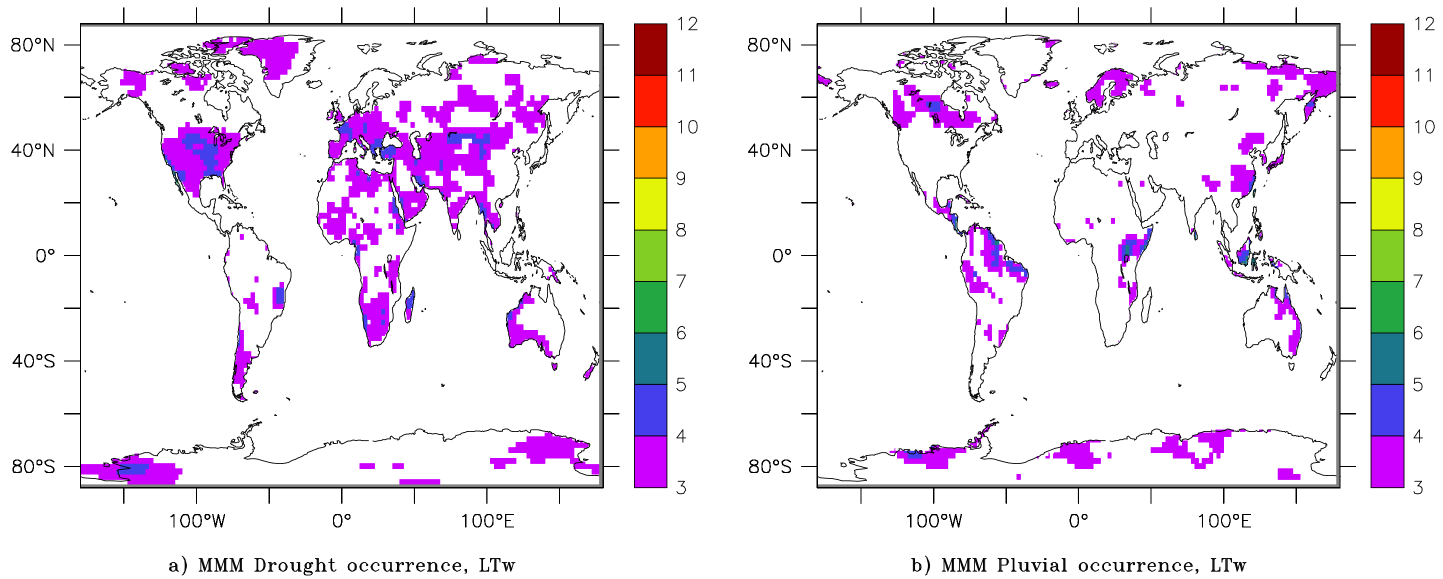

Figure 11: (a) Drought and (b) pluvial occurrence in the warm trend experiment for the MMM.